DESIGN OF BIOCHAR-NZVI/GRAPHENE NANOSHEET FOR CIPROFLOXACIN DEGRADATION

A B Wongso, B Nugroho, R Safriani, F N Faizah, N Novalia, U Sulaeman*
[1] Departement of Pharmacy, Jenderal Soedirman University,
Purwokerto, Central Java, Indonesia, 53123

Email : sulaeman@unsoed.ac.id

Abstract. The antibiotic ciprofloxacin (CIP) is a non-biodegradable pharmaceutical compound that can pollute the environment, cause microbial resistance, and disrupt the photosynthesis process. Waste containing this material must be degraded before being discharged into the environment. A material that is quite promising for degrading the antibiotic ciprofloxacin is biochar-nZVI/graphene nanosheet. Biochar-nZVI/graphene nanosheet was successfully synthesized using the starting materials of rice husk, iron sulfate heptahydrate, and graphite to prepare biochar, nZVi, and graphene nanosheet, respectively. The composite product formed from these three components, biochar-nZVI/graphene nanosheet, was characterized using XRD, FTIR, and SEM-EDX. The synthesized product was tested for degradation of the antibiotic ciprofloxacin by activating persulfate (PS) from peroxydisulfate (PDS). The results show that biochar-nZVI/graphene nanosheet can significantly degrade the antibiotic ciprofloxacin. The radical species $\bullet SO_4^-$ and $\bullet OH$ play an important role in the degradation of this antibiotic.

1. Introduction

Covid-19 is a disease caused by the SARS-CoV-2 virus. The virus operates by attacking the respiratory system and can lead to complications [1]. One of the antibiotics that can be used in the treatment of Covid-19 is ciprofloxacin. This antibiotic can be used to treat respiratory tract infections, pneumonia, and some symptoms arising from Covid-19 infection [2]. The World Health Organization (WHO) reports a 91% increase in global antibiotic use and a 165% increase in developing countries. Research on the content of several antibiotics in wastewater conducted post-pandemic shows that ciprofloxacin has a high intensity in water. This intensity indicates an estimated concentration of ciprofloxacin as the highest antibiotic compound in water 3. The increased use of antibiotics without proper waste treatment can increase the potential for antibiotic pollution. This antibiotic pollution will enter water bodies and pose a very dangerous impact by causing bacteria to become resistant [3]. The level of ciprofloxacin waste needs to be degraded using effective adsorbents because it can cause water environmental pollution that can endanger the ecosystem and human health.

Nanoscale Zero Valent Iron (nZVI) is a zero-valent iron nanomaterial that can be utilized for water remediation. This nanomaterial plays a role in environmental rehabilitation and the remediation of sites contaminated by organic compounds and heavy metals through persulfate (PS) activation. Its advantage lies in its high specific surface area, effectively activating persulfate to produce sulfate and hydroxyl radicals crucial in pollutant degradation [4]. However, nZVI has drawbacks, such as being easily oxidized and prone to agglomeration. Efforts to address these shortcomings include surface modification with surfactants and the addition of supports like clay minerals and zeolite, but these methods involve complex planning and high costs [5]. Therefore, a simple and cost-effective alternative is highly desirable.

nZVI can be modified using biochar, a solid material rich in carbon produced by burning organic materials or biomass with little or no oxygen (pyrolysis). Modifying biochar with nZVI has several advantages, including enhancing nanoparticle stability and dispersion, increasing specific surface area, rich in pores, strength, and abundant surface functional groups [6]. Biochar modified with nZVI produces different adsorption effects and pollutant mechanisms due to its physicochemical properties.

In situ chemical oxidation technology (ISCO) based on peroxydisulfate (PDS) is currently a highly promising method due to its high effectiveness. PDS can be activated through heat energy, ultraviolet light, and transition metals in the form of highly reactive sulfate radicals (SO4•-). Fe^{2+} is commonly chosen to activate PDS compared to other metals due to its environmental friendliness and cost-effectiveness. However, Fe^{2+} is not easily regenerated and needs to be converted to Fe^{3+}, usually done under acidic conditions to avoid iron precipitation at high pH [7]. The drawbacks can be overcome by adding graphene nanosheets as an efficient peroxydisulfate (PDS) activator, thanks to its high reactivity. Combining graphene nanosheets (GN) with nano-carbon materials like biochar produces a nanohybrid structure with higher catalytic activity [8].

Based on the information above, the synthesis of a composite consisting of three components—biochar, nZVI, and graphene nanosheet (GN)—in a peroxydisulfate system will result in an effective antibiotic degradation material. The biochar-nZVI/GN composite in this study is synthesized using waste biomass biochar, specifically rice husks, to degrade ciprofloxacin through PDS activation, producing radicals crucial in oxidizing antibiotic pollutants.

2. Methods

2.1.Chemicals

The reagents and chemicals used in the experiment and soil analysis were all of analytical grade (AR). These chemicals were employed without any prior purification unless otherwise specified.

2.2. Preparation of Biochar-nZVI/graphene nanosheet

A total of 200 g of rice husks were weighed and then washed to remove dust and attached impurities. The rice husks were then dried in an oven at 80°C for 12 hours. Afterward, the rice husks were transferred to a furnace in anaerobic conditions, and a heating process was carried out at 450°C for 4 hours. The resulting biochar was then ground and filtered through a 0.25 mm mesh. The biochar was soaked in 8 M H_2SO_4 with magnetic stirring for 6 hours to eliminate impurities and total ash content. The soaked product was washed with deionized water until reaching a neutral pH, then dried at 60°C for 12 hours in an oven. This process yielded biochar [9].

The synthesis of graphene was performed using the Hummers method, involving two stages: pre-oxidation and oxidation. In the pre-oxidation stage, the materials used were 40 mL of 8.5 g of H_2SO4, P_2O_5 (diphosphorus pentoxide), and 200 g of graphite powder. The procedure began with adding 40 mL of H_2SO_4 into an ice bath, followed by the addition of 8.5 g of $K_2S_2O_8$ and stirring. Next, 8.5 g of P_2O_5 (pentoxide) were added and stirred. Then, 200 g of graphite powder were introduced into the mixed solution for a reaction in a water bath at 80°C for 4 hours, followed by cooling with deionized water and standing for 12 hours. Subsequently, it was washed with deionized water and dried in a dryer at 60°C.In the oxidation stage, 10 g of pre-oxidized powder, 40 g of $KMnO_4$, and 5 g of $NaNO_3$ were dissolved in 230 mL of concentrated H_2SO_4 and reacted at a temperature below 20°C. The solution was homogenized at 40°C in a water bath for 4 hours. The resulting product was cleaned with deionized water in stages at temperatures below 90°C, followed by treatment at 90°C for 1 hour. The solution was lifted, and 1500 mL of deionized water was added, stirred for 15 minutes, supplemented with 50 mL of H_2O_2, stirred in oscillation for 2 hours at room temperature, and cleaned with 10% HCl until neutral. The solution was filtered and washed with deionized water until neutral, then dried at 80°C for 4 hours. Ultrasonic cleaning was performed for 2 hours at 50°C to produce a yellowish dispersion of graphene oxide (GO). The dispersion was filtered and dried in an oven [10].

2 g of biochar and 1 gram of graphene were dissolved in 100 mL of deionized water. A total of 4 g/mL of $FeSO_4.7H_2O$ with a Fe:C ratio of 4:1 was added, followed by the addition of $NaBH_4$ at a 1:1 ratio with Fe. The obtained precipitate was washed with distilled water and ethanol in 2-3 repeated cycles. Finally, the catalyst was dried in a vacuum desiccator for 24 hours. The catalyst underwent variations with graphene at 0%, 50%, and 75% [11].

2.3. Physicochemical property characterization of Biochar-nZVI/graphene nanosheet

Biochar-nZVI/GN samples with biochar content of 0%, 25%, 50%, and 75% were characterized using FTIR to examine their structure and functional groups. The morphology and particle size of the biochar-nZVI/GN with the highest capacity were characterized using SEM-EDX, and XRD analysis was performed to assess crystallinity.

2.4. Ciprofloxacin (CIP) removal

Samples of biochar, nZVI, and biochar-nZVI/GN with biochar content of 0%, 25%, 50%, and 75% were tested for their ability to degrade ciprofloxacin through the addition of peroxydisulfate. The ciprofloxacin degradation experiment was conducted in a 150 mL Erlenmeyer flask using 50 mL of ciprofloxacin solution (10 mg/L). Synthesized catalysts, 0.1 g, and 0.056 g of peroxydisulfate were added to the ciprofloxacin solution in the flask, which was then placed on a shaker bath (150 rpm). At specific time intervals, the samples were cooled and filtered. The initial reaction time was determined, and the synthesized materials were added. The concentration of ciprofloxacin was determined using a UV-Vis spectrophotometer at a wavelength of 277.9 nm, a predetermined wavelength before the experiment.

3. Results And Discussion

3.1. Biochar-nZVI/graphene nanosheet characterization

3.1.1 FT-IR and optical studies

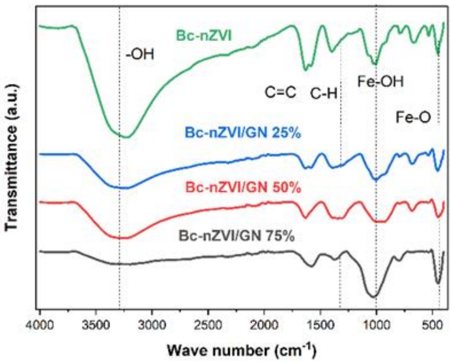

Figure 1. FT-IR Spectra

Those functional groups exhibit main peaks, namely -OH; C=C; -C-H; Fe-OH; and Fe-O. These peaks serve as references for the successful impregnation of active and conductive elements into the biochar support. Based on Figure 1, the FTIR spectrum shows the -OH group, with the peak identifying the biochar at around 3200 cm^{-1} representing the vibration of this -OH group [12]. In the catalyst variations, with the addition of graphene, the absorption peaks of the -OH group become flatter. In Bc-nZVI/GN 25%, the range is ~3251 cm^{-1}, in Bc-nZVI/GN 50% ~3248 cm^{-1}, and in Bc-nZVI/GN 75% ~3230 cm^{-1}. This indicates the presence of hydroxyl and adsorbed water in biochar [12]. Additionally, biochar is indicated by the peaks of aliphatic -CH long-chain in variations BC-nZVI at 1375 cm^{-1}, in BC-nZVI/GN 25% at 1339.54 cm^{-1}, in BC-nZVI/GN 50% at 1390.01 cm^{-1}, and in BC-nZVI 75% at 1395.48 cm^{-1}. These peaks show flattening, indicating the replacement by graphene groups [8].

The vibrational framework of the aromatic C=C group indicates the presence of carbon-rich graphene groups [13]. In BC-nZVI/GN 25%, the absorption is at 1581.97 cm^{-1}, in Bc-nZVI/GN 50% at 1632.29 cm^{-1}, and in Bc-nZVI/GN 75% at 1630.35 cm^{-1}. This suggests a decrease in the intensity of the carbonyl group on the biochar surface due to the accommodation of graphene [14]. The Fe—OH vibration group is observed at 1025.77 cm^{-1} in BC-nZVI, in BC-nZVI/GN 25% at 887.05 cm^{-1}, in Bc-nZVI/GN 50% at 1004.54 cm^{-1}, and in Bc-nZVI/GN 75% at 1006.86 cm^{-1}. The bending of the Fe-O group is present at 451.80 cm^{-1} in BC-nZVI, in BC-nZVI/GN 25% at 451.68 cm-1, in Bc-nZVI/GN 50% at 453.81 cm^{-1}, and in Bc-nZVI/GN 75% at 451.89 cm^{-1}. The characterization of iron (Fe) from the Fe-O and Fe-OH groups indicates the presence of nZVI in the synthesized composite [15].

3.1.2. Crystalline structure of Biochar-nZVI/graphene nanosheet

XRD analysis was conducted to determine the crystallinity of the composite, with the XRD measurement selected for the most effective degradation ability. The results of the XRD analysis are shown in Figure 2.

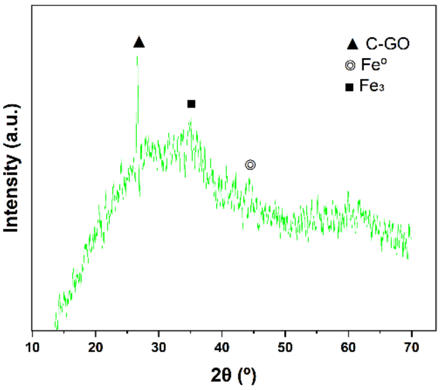

Figure 2. X-ray diffraction patterns

Figure 2 exhibited the diffractogram of small peaks at 44.37° and 35.1°. These peaks were assigned to nZVi (Fe^o) and iron oxide (Fe_3O_4), respectively. These correspond to the crystal of Fe^o (110) planes, and Fe3O4 (311) planes [16]. Fe3O4 forms an oxide shell around nZVI [17]. Based on the Scherer method the crystal sizes of 3.93 nm and 3.81 nm could be obtained in nZVI (Fe^o) and iron oxide. The carbon peak of graphene appears at 2θ, 26.6° with a size of 3.74 nm. An amorphous form of XRD profile might be associated with inorganic carbon derived from graphene [18].

3.1.3. Physical morphology and chemical composition of Biochar-nZVI/graphene nanosheet

Characterization was carried out through SEM-EDS observations, where SEM was used to examine the surface morphology of the catalyst, as presented in Figure 3, and EDS was used to observe the element distribution, as shown in Figure 4.

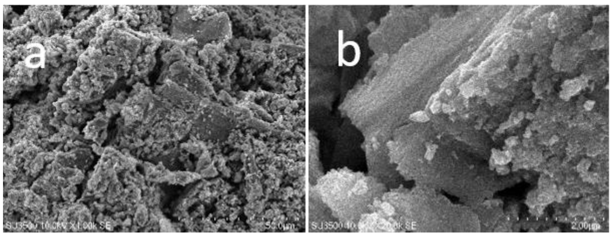

Figure 3. (a) SEM (Scanning Electron Microscope) Magnification 1k and (b) SEM Magnification 20k

Figure 3 presents the results of SEM mapping at (a) 1k magnification and (b) 20k magnification. The Scanning Electron Microscope (SEM) analysis of the synthesized composite, after stability, agglomeration, and reduction stages, in Figure 4.4(a), reveals a uniformly structured surface with rod-shaped micropores of biochar partially covered by graphene sheets forming a continuous membrane. The graphene layers encapsulate the pores, and in Figure 4.4(b), nZVI forms distributed clusters on the surface [18]. Numerous nZVI particles are dispersed on the graphene surface, but after the cleaning process with deionized water, the distribution of nZVI particles decreases 10. Based on these observations, the composite exhibits an aggregated form. This aggregation is due to the conductivity and activity of nZVI, which has magnetic properties and high attraction between nZVI, resulting in a chain-like structure [19.].

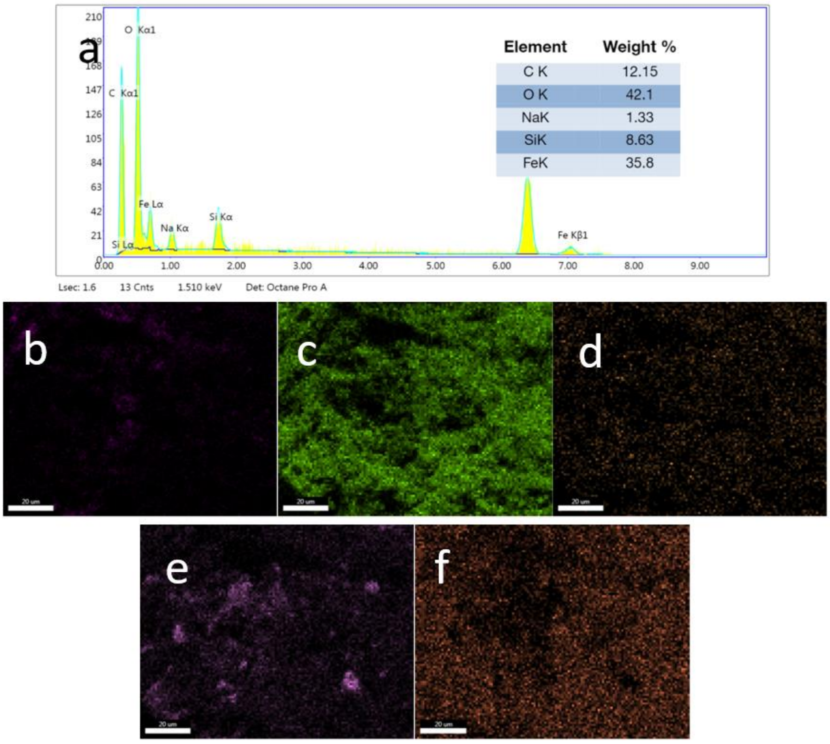

Element	Weight %
C K	12.15
O K	42.1
NaK	1.33
SiK	8.63
FeK	35.8

Figure 4. (a) EDS Analysis, (b) C Element Mapping, (c) O Element Mapping, (d) Na Element Mapping, (e) Si Element Mapping, (f) Fe Element Mapping

Based on the EDS mapping, the elements of the composite in Figure 4(a) are indicated, showing the presence of carbon, oxygen, sodium, silicon, and iron, with respective compositions in the spectrum of 5%, 54%, 3%, 19%, and 18%. These elements demonstrate the successful conjugation and functionalization in the composite fabrication [17]. The mapping results in Figure 4(b) for carbon (C) show partial dispersion and some accumulation, in Figure 4(c) for oxygen (O), a dense surface with the highest composition, in Figure 4.5(d) for sodium (Na), scattered atom distribution, in Figure 4(e) for silicon (Si), partial clustering and some dispersion, and in Figure 4(f) for iron (Fe), diverse and dispersed particles.

3.2. CIP removal from aqueous solution by Biochar-nZVI/graphene nanosheet

The degradation process has been successfully carried out with an achievement of 100%. The degradation of Ciprofloxacin by Peroxydisulfate (PDS) activated by Bc-nZVI/GN was performed for each catalyst variation, namely BC-nZVI, BC-nZVI/GN 25%, BC-nZVI/GN 50%, and BC-nZVI/GN 75%. The degradation process was conducted in a batch system, and each catalyst was measured every 10 minutes of reaction time. The degradation results of each synthesis are presented in Figure 5.

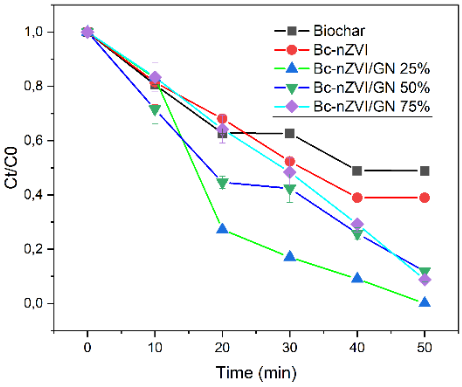

Figure 5. Ciprofloxacin Degradation Activity

Figure 5 illustrates the Ciprofloxacin degradation activity. Based on Figure 5, the most effective catalyst was found to be in the BC-nZVI/GN 25% variation, with a degradation efficiency reaching 99.98%. In its degradation, porous biochar can remove Ciprofloxacin through adsorption, as seen in the measurements that show similar results in the first 10 minutes. However, subsequent minutes significantly demonstrate significant degradation, indicating the activation of persulfate by nZVI. This result indicates that Ciprofloxacin can be removed through adsorption by biochar and due to the radical oxidation from persulfate in the BC-nZVI/GN system [15].

3.2.1. Physiochemical stability of Biochar-nZVI/graphene nanosheet

Catalyst stability testing was conducted through repeated use, using the most effective catalyst, namely the BC-nZVI/GN 25% variation. The reaction was performed for three cycles, and the results of the testing are shown in Figure 6. The catalyst's activity in the first and second cycles showed almost no change, with consecutive degradation effectiveness of 99.98% and 99.95%. The third repetition demonstrated an effectiveness of 92.49%, with no significant changes.

These results indicate good catalyst stability and its usability for multiple degradation cycles [20].

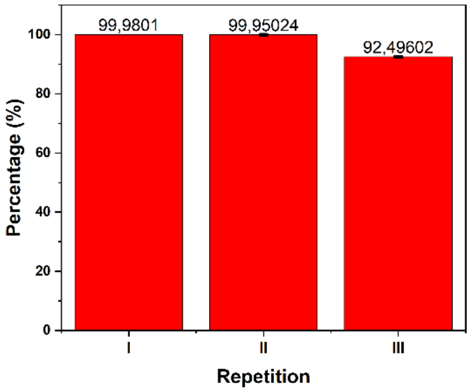

Figure 6. Performance of Bc-nZVI/GN 25% for CIP removal after regeneration

3.2.2 CIP removal mechanism

Based on the results above and literature studies, the mechanism of Ciprofloxacin degradation by persulfate activated by Bc-nZVI/GN can be illustrated in Figure 7.

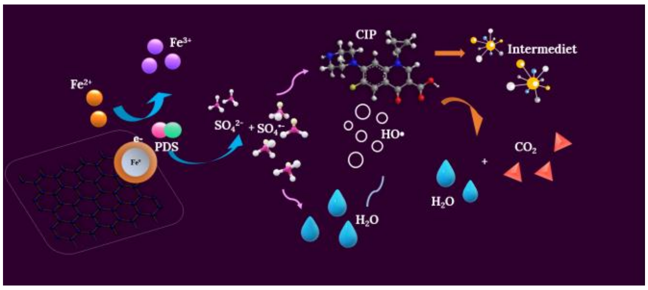

Figure 7. Degradation Mechanism of Ciprofloxacin.

In Figure 7, the removal of Ciprofloxacin (CIP) can be achieved by reactive radical species $SO_4\,\bullet^-$ and OH• through the activation of peroxydisulfate (PDS), forming intermediate compounds from CIP and producing water molecules (H2O) and carbon dioxide (CO_2). On the other hand, the use of nZVI undergoes oxidation, resulting in the conversion of Fe^{2+} to Fe^{3+} [21].

4. Conclusion

The binding of nZVI and GO nanoparticles to biochar prevents aggregation and direct oxidation while maintaining the reactivity of active nZVI and providing stability. XRD analysis results show that nZVI has a diffraction pattern at the peak of 44.37º with a crystallite size of 3.93 nm. FTIR analysis reveals functional groups such as -CH for surface biochar identification and C=C aromatic for identifying graphene as carbon and bends of Fe-O and Fe-OH identify the presence of nZVI. The degradation activity results show an effectiveness of 99.98% in CIP degradation.

5. Acknowledgment

This research was financially supported by the Directorate General of Higher Education, Research and Technology, Ministry of Education, Culture, Research and Technology through the Student Creativity Program.

References

[1]. Levani P, Prasetya AD, Mawaddatunnadila S. (2021).Coronavirus Disease 2019 (COVID-19): Patogenesis, Manifestasi Klinis dan Pilihan Terapi. J Kedokteran dan Kesehatan. 17(1):44-57. https://jurnal.umj.ac.id/index.php/JKK/article/view/6340

[2]. Kurniawan I, Mariadi PD. (2019). Analisis Potensi Cemaran Sisa Penggunaan Antibiotik di Perairan Umum (Studi Kasus : Badan Sungai Musi Kota Palembang). Sainmatika J Ilm Mat dan Ilmu Pengetah Alam.16(2):110-121. doi:10.31851/sainmatika.v16i2.3176

[3]. Farhan A, Khan NUK, Ali SMM. (2022). Assessment of Efficacy of Nimesulide in the Treatment of COVID-19 Infection. J Pharm Reseach. 34(39B):35-42. doi:10.9734/jpri/2022/v34i39B36246

[4]. Wacławek S, Lutze HV, Grübel K, Padil VV, Černík M, Dionysiou D. (2017) Chemistry of persulfates in water and wastewater treatment: a review. Chem Eng J.330:44-62.

[5]. Dan-Iya BI, Shukor MY. (2020). Modelling the Effect of Nanoscale Zero-Valent Iron (nZVI), Biochar (BC) and Nanoscale Zero-Valent Iron/Biochar (nZVI/BC) on the Adsorption/Reduction of Nitrobenzene (NB). J Environ Bioremediation Toxicol. 3(2):11-16. doi:10.54987/jebat.v3i2.545

[6]. Tang L, Yu J, Pang Y, et al. (2018). Sustainable efficient adsorbent: Alkali-acid modified magnetic biochar derived from sewage sludge for aqueous organic contaminant removal. Chem Eng J. 336:160-169. doi:https://doi.org/10.1016/j.cej.2017.11.048

[7]. Sun H, Zhang B, Wang N, et al. (2023). Refractory Organics Removal In PMS And H2O2/PMS Oxidation System Activated By Biochar/Nzvi/MoS2 Composite: Synthesis, Performance, Mechanism And Dosing Methods. J Environ Chem Eng. 11(1):367-375. doi:https://doi.org/10.1016/j.jece.2022.109134

[8]. Cruz-Alcalde A, López-Vinent N, Ribeiro RS, Giménez J, Sans C, Silva AMT. (2022). Persulfate activation by reduced graphene oxide membranes: Practical and mechanistic insights concerning organic pollutants abatement. Chem Eng J. 427(1):130994. doi:https://doi.org/10.1016/j.cej.2021.130994

[9]. Chen Q, Zhang TC, Ouyang L, Yuan S. (2022). Single-Step Hydrothermal Synthesis of Biochar from H3 PO4-Activated Lettuce Waste for Efficient Adsorption of Cd(II) in Aqueous Solution. Molecules.27(1). doi:10.3390/molecules27010269

[10]. Zhang B, Zhu BH, Wang X, You SB. (2020). Nanoscale zero valent iron supported by biomass-activated carbon for highly efficient total chromium removal from electroplating wastewater. Water (Switzerland). 12(1):1-13. doi:10.3390/w12010089

[11]. Jing Q, Qiao S, Xiao W, Tong L, Ren Z. (2021). Efficient Removal of 2,4-DCP by Nano Zero-Valent Iron-Reduced Graphene Oxide: Statistical Modeling and Process Optimization Using RSM-BBD Approach. Adsorpt Sci Technol. doi:10.1155/2021/7130581

[12]. Wang H, Zhang M, Li H. (2019). Synthesis of nanoscale zerovalent iron (nZVI) supported on biochar for chromium remediation from aqueous solution and soil. Int J Environ Res Public Health. 16(22). doi:10.3390/ijerph16224430

[13]. Fan M, Li T, Hu J, et al. (2016). Synthesis and characterization of reduced graphene oxide-supported nanoscale zero-valent iron (nZVI/rGO) composites used for Pb(II)

removal. Materials (Basel). 9(8). doi:10.3390/ma9080687

[14]. Mandal S, Pu S, He L, Ma H, Hou D. (2020). Biochar induced modification of graphene oxide & nZVI and its impact on immobilization of toxic copper in soil. Environ Pollut. 259:113851. doi:10.1016/j.envpol.2019.11385

[15]. Sponza D, Koyuncuoglu P. (2019). Photodegradation of ciprofloxacin and ofloxacin antibiotics and their photo-metabolites with sunlight. Clin Microbiol Infect Dis. 2019;4(1):1-10. doi:10.15761/cmid.1000149

[16]. Ghaffar A, Younis MN. (2014). Adsorption of organic chemicals on graphene coated biochars and its environmental implications. Green Process Synth. 3(6):479-487. doi:10.1515/gps-2014-0071

[17]. Mehrabi N, Masud A, Afolabi M, Hwang J, Calderon Ortiz GA, Aich N. (2019). Magnetic graphene oxide-nano zero valent iron (GO-nZVI) nanohybrids synthesized using biocompatible cross-linkers for methylene blue removal. RSC Adv. 9(2):963-973. doi:10.1039/C8RA08386J

[18]. Neeli ST, Ramsurn H. (2018). Synthesis and formation mechanism of iron nanoparticles in graphitized carbon matrix using biochar from biomass model compounds as a support. Carbon N Y.134:480-490. doi:10.1016/j.carbon.2018.03.079

[19]. El-shafei MM, Hamdy A, Hefny MM. (2018). Zero-valent iron nanostructures: synthesis, characterization and application. (January).

[20]. Alhindawy IG, Mira HI, Youssef AO, et al. (2022). Cobalt doped titania-carbon nanosheets with induced oxygen vacancies for photocatalytic degradation of uranium complexes in radioactive wastes. Nanoscale Adv. 4(24):5330-5342. doi:10.1039/d2na00467d

[21]. Hu C, Chen M, Wang L, et al. (2023). Dual promoted ciprofloxacin degradation by Fe0/PS system with ascorbic acid and pre-magnetization. Chemosphere. 336(139202):139-202. doi:https://doi.org/10.1016/j.chemosphere.2023.139202